⌘ *Author's Choice*

THE JOURNAL OF BIOLOGICAL CHEMISTRY VOL. 284, NO. 37, pp. 24965–24971, September 11, 2009

cAMP Stimulates Apical Exocytosis of the Renal Na^+-K^+-$2Cl^-$ Cotransporter NKCC2 in the Thick Ascending Limb

*ROLE OF PROTEIN KINASE A**

Received for publication, June 23, 2009, and in revised form, July 6, 2009 Published, JBC Papers in Press, July 10, 2009, DOI 10.1074/jbc.M109.037135

Paulo S. Caceres[‡§], Gustavo R. Ares[‡], and Pablo A. Ortiz[‡§1]

From the [‡]Hypertension and Vascular Research Division, Henry Ford Hospital, and the [§]Department of Physiology, School of Medicine, Wayne State University, Detroit, Michigan 48202

The apical renal Na^+-K^+-$2Cl^-$ cotransporter NKCC2 mediates NaCl absorption by the thick ascending limb (TAL) of Henle's loop. cAMP stimulates NKCC2 by enhancing steady-state apical membrane levels of this protein; however, the trafficking and signaling mechanisms by which this occurs have not been studied. Here, we report that stimulation of endogenous cAMP levels with either forskolin/3-isobutyl-1-methylxanthine (IBMX) or the V2 receptor agonist [deamino-Cys[1],D-Arg[8]]vasopressin increases steady-state surface NKCC2 and that the protein kinase A (PKA) inhibitor H-89 blocks this effect. Confocal imaging of apical surface NKCC2 in isolated perfused TALs confirmed a stimulatory effect of cAMP on apical trafficking that was blocked by PKA inhibition. Selective stimulation of PKA with the agonist N^6-benzoyl-cAMP (500 μM) stimulated steady-state surface NKCC2, whereas the Epac-selective agonist 8-*p*-chlorophenylthio-2′-*O*-methyl-cAMP (100 and 250 μM) had no effect. To explore the trafficking mechanism by which cAMP increases apical NKCC2, we measured cumulative apical membrane exocytosis and NKCC2 exocytic insertion in TALs. By monitoring apical FM1–43 fluorescence, we observed rapid stimulation of apical exocytosis (2 min) by forskolin/IBMX. We also found constitutive exocytic insertion of NKCC2 in TALs over time, which was increased by 3-fold in the presence of forskolin/IBMX. PKA inhibition blunted cAMP-stimulated exocytic insertion but did not affect the rate of constitutive exocytosis. We conclude that cAMP stimulates steady-state apical surface NKCC2 by stimulating exocytic insertion and that this process is highly dependent on PKA but not Epac.

The renal-specific Na^+-K^+-$2Cl^-$ cotransporter NKCC2 is expressed at the apical membrane and in subapical vesicles in the thick ascending limb (TAL)[2] of Henle's loop, where it mediates NaCl reabsorption (1). Hormonal stimulation of intracellular cAMP by arginine vasopressin enhances NaCl absorption in the TAL by stimulating NKCC2-dependent transport (2–5).

As NKCC2 must be in the plasma membrane to mediate NaCl absorption, vesicle trafficking of NKCC2, including exocytic insertion, endocytic retrieval, and recycling to and from the plasma membrane, is likely to play a major role in NKCC2 regulation. Despite its importance, the regulation of NKCC2 trafficking by cAMP has not been thoroughly studied.

We showed previously that cAMP stimulates NKCC2-dependent NaCl reabsorption by increasing steady-state surface NKCC2 in rat TALs (6). In addition, others have shown that the V2 receptor agonist [deamino-Cys[1],D-Arg[8]]vasopressin (dDAVP) increases apical membrane NKCC2 labeling in mouse TALs *in vivo* (7). These data indicate that enhanced steady-state apical surface NKCC2 levels are involved in the stimulation of NKCC2 activity and NaCl absorption caused by cAMP. However, the signaling cascade involved in the stimulation of NKCC2 trafficking has not been studied in polarized TAL cells.

In other epithelial cells, cAMP stimulates protein trafficking by activating protein kinase A (PKA) and/or Epac (guanine exchange protein activated by cAMP) (8–13). PKA is expressed in TALs and binds cAMP in response to arginine vasopressin stimulation (14). In addition to PKA, the Epac isoforms Epac1 and Epac2 are expressed in TALs (15), but their role in NKCC2 trafficking has not been addressed. In the collecting duct epithelium, arginine vasopressin and cAMP stimulate aquaporin-2 exocytic insertion into the apical membrane and enhance water permeability (16) in a process mediated by PKA (17–20). However, Epac-selective agonists also enhance aquaporin-2 trafficking and apical exocytosis in this renal epithelium, suggesting a role for Epac1 (10, 21). In addition, in other cells, Epac-dependent signaling exerts opposite effects compared with PKA (22, 23). We hypothesized that cAMP increases steady-state surface NKCC2 expression in native TALs by stimulating apical exocytosis and that PKA mediates this process. Our data show for the first time that cAMP stimulates the rate of NKCC2 exocytosis via PKA and that this trafficking step mediates the increase in steady-state surface NKCC2 in native TALs.

EXPERIMENTAL PROCEDURES

Drugs

Reagents for steady-state surface biotinylation and exocytic insertion protocols were from ThermoFisher Scientific (Waltham, MA). PKA- and Epac-selective agonists were from Biolog/Axxora (Bremen, Germany), and H-89 was obtained from EMD Chemicals (San Diego, CA) or LC Laboratories

* This work was supported, in whole or in part, by National Institutes of Health Grants R01 HL080409-05 and P01 HL090550-01 (Subproject 2; to P. A. O.).
⌘ *Author's Choice*—Final version full access.

[1] To whom correspondence should be addressed: Hypertension and Vascular Research Div., Henry Ford Hospital, E&R Bldg., Rm. 7041, 2799 W. Grand Blvd., Detroit, MI 48202. Tel.: 313-916-7164; E-mail: portiz1@hfhs.org.

[2] The abbreviations used are: TAL, thick ascending limb; dDAVP, [deamino-Cys[1],D-Arg[8]]vasopressin; PKA, protein kinase A; NHS-SS-biotin, sulfosuccinimidyl 2-(biotinamido)ethyl-1,3-dithiopropionate; e-NKCC2, extracellular NKCC2 epitope; IBMX, 3-isobutyl-1-methylxanthine.

(Woburn, MA). All fluorescent reagents, including FM1–43 and Alexa Fluor-labeled antibodies, were from Invitrogen. All other reagents were from Sigma.

Suspensions of Medullary TALs

Kidneys were obtained from 250–300-g male Sprague-Dawley rats (Charles River Breeding Laboratories, Wilmington, MA) as described (6). The outer medulla was dissected, minced, and digested in collagenase in buffer A (130 mM NaCl, 2.5 mM NaH_2PO4, 4.0 mM KCl, 1.2 mM $MgSO_4$, 6 mM L-alanine, 1.0 mM disodium citrate, 5.5 mM glucose, 2.0 mM calcium lactate, and 10 mM HEPES, pH 7.4) to obtain TAL suspensions.

Surface Biotinylation of TAL Suspensions

Steady-state Surface NKCC2—Biotinylation of TAL surface NKCC2 was performed as described in detail previously (6, 24). TALs were equilibrated at 37 °C for 15 min and then treated with vehicle or corresponding drug for 30 min. In some experiments, H-89 was present during the equilibration period. TALs were biotinylated at 4 °C with sulfosuccinimidyl 2-(biotinamido)ethyl-1,3-dithiopropionate (NHS-SS-biotin; 0.9 mg/ml); washed; and lysed in buffer containing 150 mM NaCl, 50 mM HEPES, pH 7.5, 5 mM EDTA, 1% Triton X-100, 0.1% SDS, and protease inhibitors. Biotinylated proteins were separated with streptavidin-coated beads overnight at 4 °C and recovered by boiling in Laemmli loading buffer containing dithiothreitol and β-MeEtOH. Proteins were resolved on 6% SDS-polyacrylamide gels, and NKCC2 and glyceraldehyde-3-phosphate dehydrogenase were detected by Western blotting. Control experiments showed the absence of biotinylation of glyceraldehyde-3-phosphate dehydrogenase in the surface fraction, no change in total NKCC2 with various treatments (see Fig. 1*A*), linear recovery of biotinylated NKCC2, complete extraction of biotinylated proteins from beads, and a linear range of surface NKCC2 signal in films. NKCC2 was detected with chicken anti-rat NKCC2 antibody (1:1400; raised against an N-terminal sequence of rat NKCC2) (6), and glyceraldehyde-3-phosphate dehydrogenase was detected with monoclonal antibodies from Chemicon (Temecula, CA). Bands were detected by chemiluminescence and quantified.

Exocytic Insertion of NKCC2—Surface proteins accessible to NHS-SS-biotin in TAL suspensions were first masked by reaction with membrane-impermeant NHS-acetate as described previously for other membrane proteins (25, 26). Briefly, TALs were incubated with NHS-acetate (2 mg/ml in buffer A, pH 7.8) at 4 °C for 1 h, adding fresh NHS-acetate every 15 min. The drugs for treatment were added at 4 °C, and samples were warmed to 37 °C. Exocytosed NKCC2 was chased for 15, 30, and 45 min. TALs were then cooled, and newly inserted NKCC2 was biotinylated with NHS-SS-biotin. The efficiency of NHS-acetate masking for NKCC2 was calculated in every experiment from the difference between a TAL aliquot that was not masked with NHS-acetate (100% basal surface NKCC2) and an aliquot that was masked at 4 °C but never warmed to 37 °C (0 time point). The difference between these two samples represents the NHS-acetate-masked surface NKCC2 fraction, which was used to express exocytic insertion over time. NHS-acetate consistently masked 80% of surface NKCC2 accessible for biotinylation.

Confocal Microscopy for Apical Surface NKCC2 in Microperfused TALs

Male Sprague-Dawley rats weighing 120–150 g were used for TAL perfusion as described previously (6, 24). Apical NKCC2 was measured after labeling NKCC2 in intact microperfused TALs with a rabbit antibody against a predicted extracellular epitope (4) of rat NKCC2 (e-NKCC2) as described (24). After treatment of perfused TALs with vehicle or drugs in the absence or presence of H-89 (10 μM) at 37 °C, protein trafficking was stopped by cooling TAL cells to 4 °C, and apical membranes were labeled with anti-e-NKCC2 antibody (1:100 in 2.5% bovine serum albumin, pH 7.6) added to the lumen perfusate for 30 min at 4 °C. The lumen was washed, and TALs were fixed while at 4 °C with 4% paraformaldehyde in phosphate-buffered saline. Fixed cells were blocked with 2.5% bovine serum albumin, followed by 20 min of apical labeling with Alexa Fluor 488-labeled anti-rabbit IgG highly cross-adsorbed at 1:200 in 2.5% bovine serum albumin. Undetectable labeling was observed in the absence of primary e-NKCC2 antiserum (data not shown). The e-NKCC2 antiserum was characterized previously in isolated perfused rat TALs (24). Images were acquired using a laser scanning confocal microscopy system (Visitech International) with acousto-optical tunable filter-controlled argon laser (488 nm line) excitation. Fluorescence was measured with a 500-nm long-pass filter. Identical settings were used to obtain cross-section *z*-series images from individual TAL cells along a tubule. To diminish day-to-day variation, fluorescence intensity was regularly calibrated to a linear range using FocalCheck slides. Two-dimensional image analysis was used to measure fluorescence intensity in regions of interest encompassing the apical membrane of several cells in each image. Mean fluorescence intensity was obtained for at least 14 cells/TAL tubule and averaged.

Real-time Monitoring of Apical Membrane Exocytosis in TALs

Apical exocytosis in microperfused TALs was monitored by measuring FM1–43 fluorescence of apical membranes as described previously for renal collecting ducts (10, 21). FM1–43 fluoresces when bound to membranes but not in aqueous solution and is impermeable to cell membranes. Thus, its intensity is directly related to membrane surface area and is used as an index of cumulative exocytosis (27, 28). Briefly, 2 μM FM1–43 was included in the luminal perfusate and exchanged for 30 s before imaging. FM1–43 was present in the flowing apical solution for the remainder of the experiment. Images were acquired via laser scanning confocal microscopy at a cross-section of labeled TALs along the *z* axis so that the apical membranes of TAL cells were in focus on both sides of the lumen. FM1–43 was excited with an acousto-optical tunable filter-controlled argon laser at 488 nm, and emission was collected with a 525-nm long-pass emission filter. Images were acquired for 100 ms, every 10 s. After a 10-min period with continuous FM1–43 perfusion, the dye was washed out from the lumen. We observed little endocytosis of FM1–43 prior to 10 min; however, subapical vesicles were visible after 10 min of

incubation with the dye (data not shown). Regions of interest were generated encompassing the apical and subapical spaces in each TAL image (generally four cells at each side of the tubule wall). Mean fluorescence intensity was obtained for six to eight cells/tubule and averaged.

Statistics

Results are expressed as means ± S.E. One-way analysis of variance was used to determine differences between means in different treatment groups. $p < 0.05$ was considered significant.

RESULTS

cAMP Increases Steady-state Apical Surface NKCC2 via PKA in TALs—In TALs, cAMP stimulates NKCC2-dependent NaCl reabsorption by increasing steady-state surface NKCC2 (6), but the signaling cascade mediating this effect is not clear. We first tested whether cAMP-induced stimulation of surface NKCC2 is mediated by PKA. We used forskolin (20 μM), an adenylyl cyclase agonist, plus 3-isobutyl-1-methylxanthine (IBMX; 0.5 mM), a general phosphodiesterase inhibitor, to increase intracellular cAMP. We found that incubating TALs for 30 min with forskolin/IBMX increased steady-state surface NKCC2 by 81 ± 16% ($p < 0.05$). Preincubation of TALs with the PKA inhibitor H-89 (10 μM) blocked 70% of the forskolin/IBMX effect, which only weakly stimulated surface NKCC2 ($p < 0.05$ *versus* forskolin/IBMX) (Fig. 1, *A* and *B*). In control experiments, we found no change in surface NKCC2 when TALs were incubated with either IBMX (14 ± 8%) or H-89 alone (7 ± 8%) (data not shown). To increase cAMP levels with a physiological agonist, we used the vasopressin V2 receptor agonist dDAVP. We observed that a 30-min incubation with 1 μM dDAVP increased surface NKCC2 by 23 ± 9% ($p < 0.05$). Phosphodiesterase inhibition with IBMX enhanced the effect of dDAVP, which stimulated surface NKCC2 by 44 ± 11% ($p < 0.05$). However, in TALs preincubated with H-89, the effect of dDAVP + IBMX was completely blocked (Fig. 1*C*). These data indicate that PKA mediates the stimulatory effect of cAMP on steady-state surface NKCC2.

To directly image the effect of cAMP on apical membrane NKCC2 levels, we used immunofluorescence and confocal microscopy in perfused TALs. To detect surface NKCC2 in the apical membrane but not in the intracellular pool, we labeled the apical side of intact TALs with an antibody against an extracellular NKCC2 sequence located between the TM5 and TM6 domains facing the apical side, as described under "Experimental Procedures." In control TALs incubated with vehicle, we found the expected NKCC2 labeling along the apical surface of all TAL cells (Fig. 2*A*). In TALs treated with forskolin/IBMX for 30 min, apical NKCC2 labeling was increased by 75% (from 151 ± 10 to 263 ± 15 fluorescence units, $p < 0.01$). However, in TALs preincubated with H-89, forskolin/IBMX (30 min) did not change apical NKCC2 labeling (139 ± 9 *versus* 142 ± 7 fluorescence units, not significant) (Fig. 2*B*). These data confirm the surface biotinylation results showing that PKA is essential for cAMP-stimulated apical NKCC2 trafficking in native TALs.

PKA- but Not Epac-selective Agonists Increase Steady-state Surface NKCC2 in TALs—To differentiate the role of PKA from the possible upstream or downstream actions of Epac, we studied the effect of a PKA-selective agonist and an Epac-selective agonist on steady-state surface NKCC2. A 30-min incubation of TALs with the PKA-selective agonist N^6-benzoyl-cAMP (0.5 and 1 mM) increased surface NKCC2 by 55 ± 26 and 95 ± 26%, respectively ($p < 0.05$), and this effect was largely abrogated in the presence of H-89 (Fig. 3). To selectively stimulate Epac signaling, we used the agonist 8-*p*-chlorophenylthio-2′-*O*-methyl-cAMP at two concentrations (100 and 250 μM). We found that a 30-min incubation with the Epac analog had no effect on surface NKCC2 levels in TALs (Fig. 3). These data suggest that PKA is the primary cAMP target mediating the stimulatory effect on NKCC2 trafficking.

cAMP Stimulates Cumulative Apical Membrane Exocytosis in TALs—The trafficking step affected by cAMP and the kinetics of NKCC2 trafficking have not been studied. NKCC2 is located in the apical membrane and subapical vesicles of TALs. To study whether cAMP stimulates apical membrane exocytosis in TALs, we monitored the effect of forskolin/IBMX on FM1–43 fluorescence in the apical membrane of microperfused TALs. FM1–43 is a styryl dye that is impermeable to cell membranes and fluoresces when bound to membranes but not in aqueous solution. Thus, its intensity is directly related to membrane surface area and is used as an index of cumulative exocytosis (27–29). TALs were perfused with luminal solution containing FM1–43 (2 μM) for 10 min, and then the luminal solution was exchanged to wash out the dye from apical membranes. Confocal images were acquired every 10 s and later analyzed to quantify apical membrane FM1–43 intensity over time in TALs treated with vehicle (basal) or forskolin/IBMX. Under basal conditions, apical FM1–43 intensity was stable and did not increase over time for a period of 10 min (Fig. 4). After washout of FM1–43 from the TAL lumen, fluorescence intensity was almost completely eliminated, indicating that little FM1–43 was internalized via endocytosis. In TALs treated with forskolin/IBMX, we observed a rapid increase in FM1–43 fluorescence intensity after 2 min (22 ± 6%, $p < 0.01$), followed by a sustained increase with a maximal difference of 47 ± 7% ($p < 0.001$) by 7 min (Fig. 4*B*). Incubation times longer than 10 min resulted in internalization of the dye and were not studied (data not shown). These data indicate that cAMP stimulates apical exocytosis in native TALs.

cAMP Stimulates Exocytic Insertion of NKCC2 in TALs—We next studied the effect of cAMP on exocytic insertion of NKCC2 in TALs. For this, we used a modified surface biotinylation protocol (25, 26) to measure exocytic insertion of NKCC2 after masking accessible biotinylation sites with NHS-SS-acetate as described under "Experimental Procedures." First, we observed constitutive NKCC2 exocytosis under basal conditions during a time course of 45 min (Fig. 5, *A* and *B*). Control experiments showed that NHS-acetate masked surface NKCC2 biotinylation by 80% (see "Experimental Procedures" for a detailed description). In paired experiments, we treated TALs with either vehicle or forskolin/IBMX and measured NKCC2 insertion after 15, 30, or 45 min. We observed that the rate of NKCC2 exocytosis was enhanced by 3-fold at 15 min,

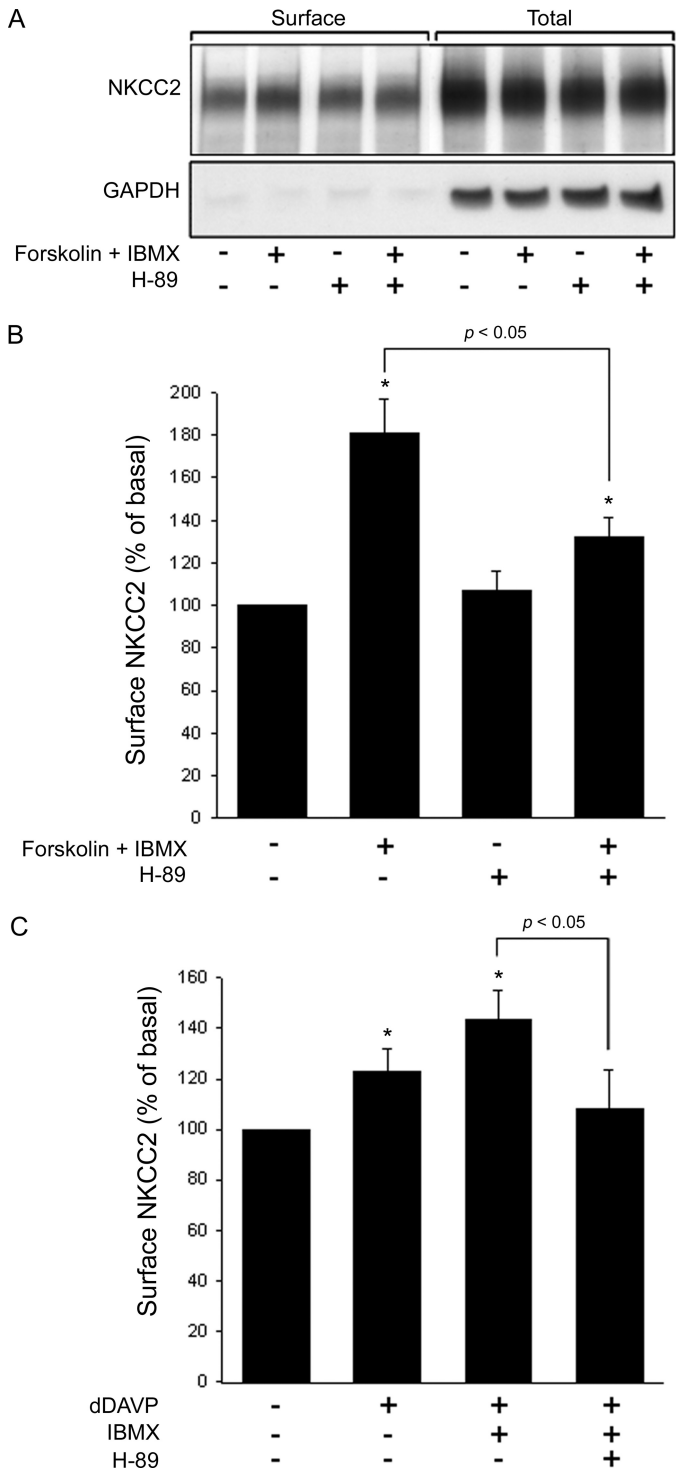

FIGURE 1. **Endogenous cAMP stimulates steady-state surface NKCC2 via PKA in TALs.** *A*, a representative Western blot shows NKCC2 steady-state surface biotinylation in TAL suspensions after 30 min of treatment with vehicle, forskolin (20 μM) plus IBMX (0.5 mM), the PKA inhibitor H-89 (10 μM), and H-89 plus forskolin/IBMX. Total NKCC2 levels measured for every experiment did not change with treatments. Control intracellular glyceraldehyde-3-phosphate dehydrogenase (*GAPDH*; *lower panel*) was not detected in the surface fraction, indicating the absence of intracellular protein biotinylation with NHS-SS-biotin as described under "Experimental Procedures." *B*, steady-state surface NKCC2 was measured in rat TAL suspensions incubated for 30 min at 37 °C with forskolin/IBMX in the absence or presence of H-89 (10 μM) ($n = 10$; *, $p < 0.05$ *versus* basal conditions). *C*, steady-state surface NKCC2 was measured in rat TAL suspensions incubated for 30 min at 37 °C with dDAVP (1 μM) in the absence or presence of IBMX (0.5 mM) and H-89 (10 μM) ($n = 5$; *, $p < 0.05$ *versus* basal conditions). After treatment, TALs were cooled to 4 °C, and steady-state surface NKCC2 was measured by biotinylation as described under "Experimental Procedures." Surface NKCC2 was detected by Western blotting, and mean optical density was measured by densitometry. Values are expressed as the mean percentage of basal levels (vehicle-treated), and *error bars* represent ± S.E.

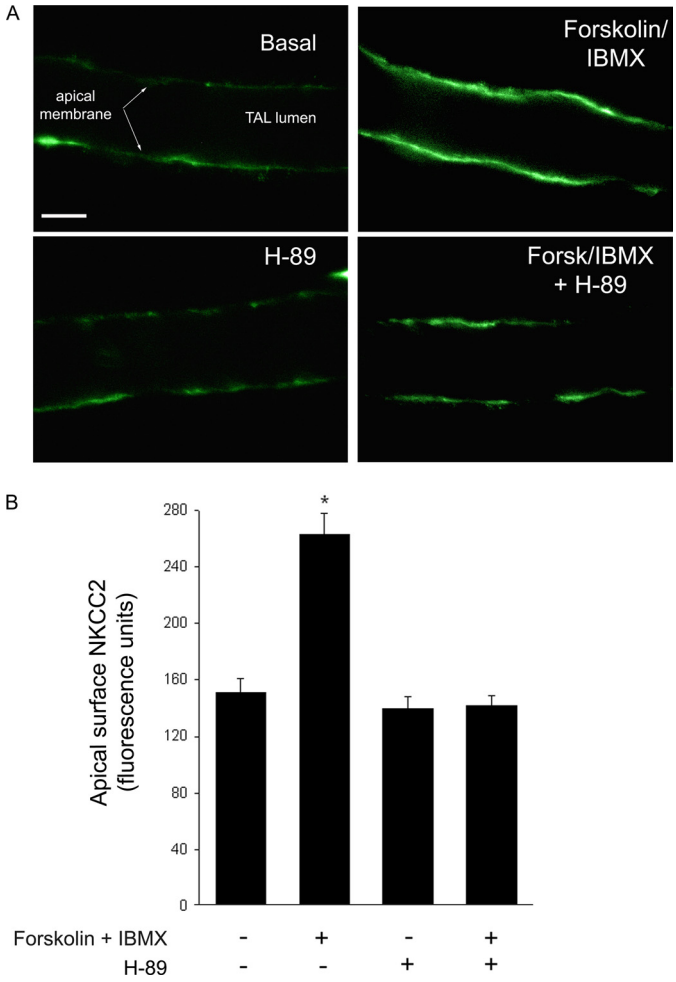

FIGURE 2. **Endogenous cAMP increases apical surface NKCC2 via PKA in isolated perfused TALs.** *A*, representative fluorescent images of apical surface NKCC2 in isolated perfused TALs. TALs were microdissected from rat kidneys and perfused at 37 °C. Either vehicle (*Basal*) or forskolin (20 μM) and IBMX (0.5 mM) were added to the bath and incubated for 30 min. In different experiments, TALs were preincubated with H-89 (10 μM) for 15 min, and then either forskolin/IBMX (*Forsk/IBMX + H-89*) or vehicle was added to the bath for 30 min. TALs were cooled to 4 °C, and apical surface NKCC2 was labeled with a rabbit antibody raised against an extracellular epitope in NKCC2 present in the luminal perfusate as described under "Experimental Procedures." Primary antibody was then labeled with Alexa Fluor 488-labeled goat anti-rabbit IgG. Fluorescent images were acquired by laser scanning confocal microscopy, and mean fluorescence intensity was measured in regions of interest at the apical membrane. *Scale bar* = 10 μm. *B*, cumulative data for steady-state apical surface NKCC2 in isolated perfused TALs treated with vehicle, forskolin/IBMX, H-89, and H-89 plus forskolin/IBMX. Two-dimensional image analysis was used to measure fluorescence intensity in regions of interest encompassing the apical membrane of at least 14 cells/TAL tubule and averaged ($n = 72–82$ cells from five independent tubules/treatment; *, $p < 0.05$ *versus* vehicle). Values are expressed as mean fluorescence arbitrary units, and *error bars* represent ± S.E.

2.8-fold at 30 min, and 2.5-fold at 45 min ($p < 0.01$) (Fig. 5*C*). These data show for the first time that cAMP stimulates the rate of NKCC2 exocytic insertion in epithelial cells.

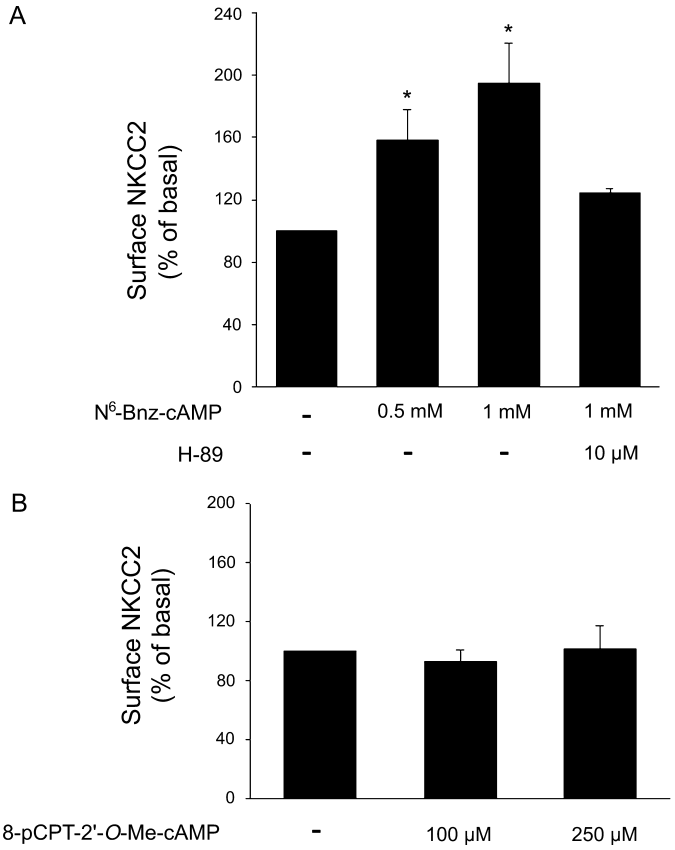

FIGURE 3. **Steady-state surface NKCC2 is increased by the PKA-selective agonist N^6 -benzoyl-cAMP but not by the Epac-selective agonist 8-*p*-chlorophenylthio-2′-*O*-methyl-cAMP.** *A*, TALs were treated for 30 min at 37 °C with the PKA-selective agonist N^6-benzoyl-cAMP (N^6-*Bnz-cAMP*) at 0.5 and 1 mM in the absence and presence of H-89 (10 μM), and steady-state surface NKCC2 was measured ($n = 7$; *, $p < 0.05$ *versus* basal conditions). *B*, TALs were treated for 30 min at 37 °C with the Epac-selective agonist 8-*p*-chlorophenylthio-2′-*O*-methyl-cAMP (*8-pCPT-2′-O-Me-cAMP*) at 100 and 250 μM ($n = 7$). After treatment, suspensions were cooled to 4 °C, and steady-state surface NKCC2 was measured by biotinylation as described under "Experimental Procedures." Surface NKCC2 was detected by Western blotting, and mean optical density was measured by densitometry. Values are expressed as the mean percentage of basal levels (vehicle-treated), and *error bars* represent ± S.E.

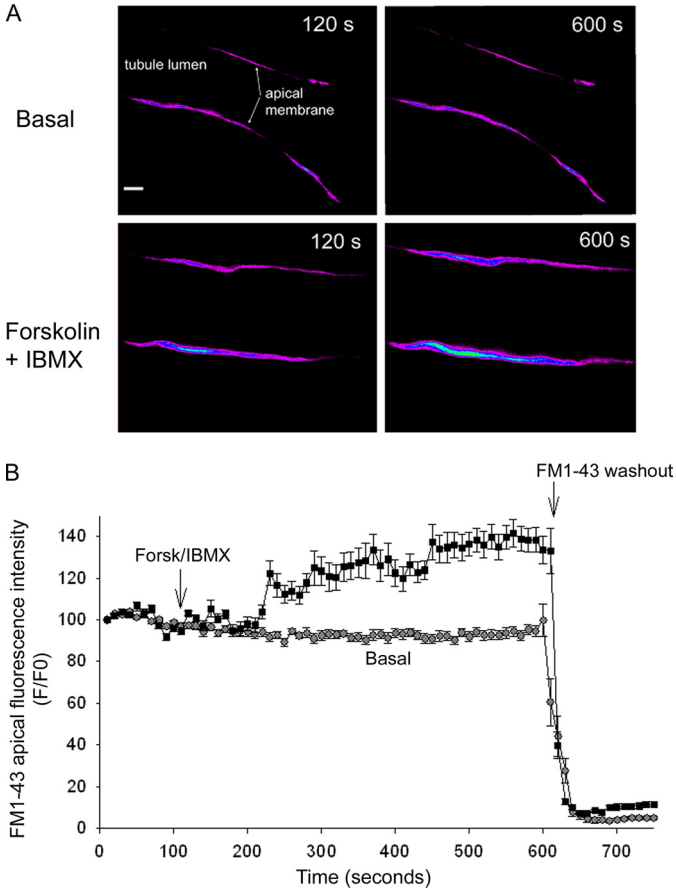

FIGURE 4. **Endogenous cAMP stimulates apical membrane exocytosis in isolated perfused TALs as measured by FM1–43 fluorescence.** *A*, representative confocal images of microperfused TALs in the presence of apical FM1–43 (2 μM) before (120 s) and after the addition of vehicle (*Basal*) or forskolin (20 μM) plus IBMX (0.5 mM) after 600 s. (Only apical membranes in focus are visible as expected from selective apical loading of FM1–43.) Images were pseudocolored with a rainbow scale; *purple* indicates low intensity, and *blue-green* indicates higher intensity. As detailed under "Experimental Procedures," enhanced fluorescence intensity is indicative of increased membrane surface area, which is correlated with enhanced apical exocytosis. *Scale bar* = 5 μm. *B*, cumulative data for FM1–43 fluorescence intensity over time normalized to initial intensity (F_0) in TALs treated with vehicle (*Basal*) or forskolin/IBMX (*Forsk/IBMX*) (*arrow*). Images were acquired every 10 s for 10 min in the presence of apical FM1–43 (2 μM). After 10 min, the dye was washed out to determine internalized FM1–43 (*FM1–43 washout*). As shown in the cumulative data, 1 min washout almost completely eliminated FM1–43 signal, indicative of little apical endocytosis. Mean fluorescence intensity was measured in regions of interest encompassing the apical membrane of at least four to six cells/tubule ($n = 22$ cells from five independent tubules/treatment).

PKA Is Involved in cAMP-stimulated but Not Constitutive Exocytic Insertion of NKCC2—PKA inhibition prevented most of the cAMP-induced increase in steady-state surface NKCC2 (Figs. 1, *A* and *B*, and 2). If exocytic insertion is the primary trafficking step required to enhance surface NKCC2, then PKA inhibition should block exocytosis. To test this, we incubated TALs with H-89 in the absence and presence of forskolin/IBMX and then measured NKCC2 exocytic insertion for 30 min. Forskolin/IBMX stimulated NKCC2 exocytic insertion compared with vehicle-treated TALs ($p < 0.05$), and H-89 blocked the stimulatory effect of forskolin/IBMX by almost 60% ($p < 0.02$) (Fig. 6). Interestingly, constitutive NKCC2 insertion was not affected by PKA inhibition. These data indicate that PKA is involved in cAMP-stimulated NKCC2 exocytosis but not in constitutive NKCC2 insertion into the apical membrane.

DISCUSSION

We found previously that cAMP stimulates NaCl absorption by TAL by increasing surface NKCC2 levels (6). However, the trafficking steps and the signaling cascade by which cAMP increases apical NKCC2 in epithelial cells were unknown. Here, we observed that PKA inhibition blocks cAMP-induced increases in steady-state surface NKCC2 when cAMP is increased by either forskolin/IBMX or the physiological agonist dDAVP in native TAL epithelium (Figs. 1 and 2). Consistent with a role of PKA, a PKA-selective agonist stimulated surface NKCC2 to similar levels compared with forskolin/IBMX, whereas the Epac-selective agonist 8-*p*-chlorophenylthio-2′-*O*-methyl-cAMP had no effect on surface NKCC2 (Fig. 3). The absence of an effect of the Epac analog may indicate that Epac is not involved in the stimulation of surface NKCC2 or that the concentration of agonist was not sufficient to stimulate Epac activity. However, the latter is unlikely because the concentra-

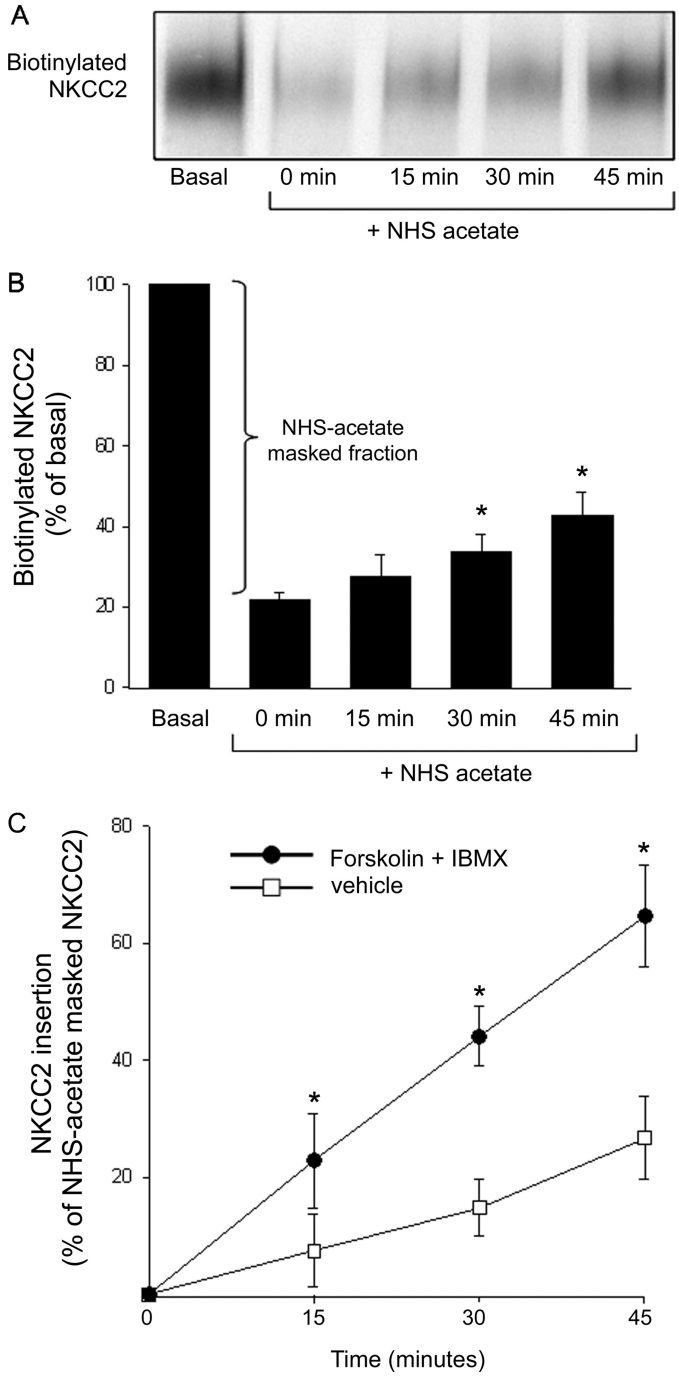

FIGURE 5. **NKCC2 exhibits constitutive exocytic insertion in TALs that is stimulated by cAMP.** *A*, a representative Western blot shows surface (biotinylated) NKCC2 expression in TALs before (*first lane*; basal surface NKCC2) and after (*second lane*; 0 min at 37 °C) treatment with NHS-acetate to mask surface biotinylation sites. After masking, TALs were incubated for 0 (*second lane*), 15 (*third lane*), 30 (*fourth lane*), and 45 (*fifth lane*) min at 37 °C to allow protein trafficking. TALs were cooled, and newly inserted NKCC2 was biotinylated and detected by Western blotting. *B*, cumulative data are shown for the exocytic insertion protocol in TAL suspensions. Constitutive NKCC2 insertion over time was observed after masking surface-accessible sites with NHS-acetate and warming to 37 °C for 0, 15, 30, and 45 min. Data are expressed as percent of the basal surface NKCC2 signal (100%), which was not masked by NHS-acetate. The difference between basal and NHS-acetate-masked TALs was considered the NHS-acetate-masked surface NKCC2 fraction, which was used to express exocytic insertion over time. Values are expressed as the mean after normalizing to basal levels (100%), and *error bars* are ± S.E. ($n = 7$; *, $p < 0.05$ *versus* 0-min time point). *C*, TAL suspensions were aliquoted, masked with NHS-acetate, and incubated at 37 °C for 0, 15, 30, and 45 min in the presence and absence of forskolin (20 μM) and IBMX (0.5 mM). One sample was not masked with NHS-acetate in every experiment (not shown). Surface NKCC2 was detected by Western blotting, and mean optical density was measured by densitometry. Data are expressed as percent of the NHS-acetate-masked fraction over time as mean ± S.E. ($n = 7$; *, $p < 0.05$ *versus* vehicle).

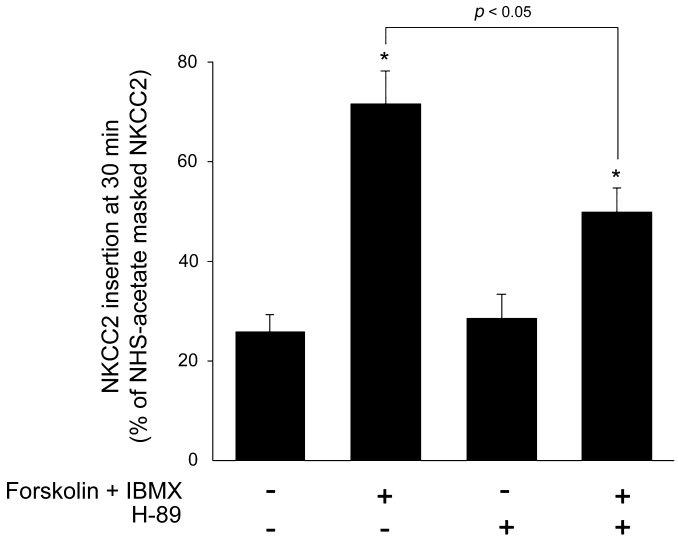

FIGURE 6. **cAMP increases the rate of NKCC2 exocytic insertion via PKA in TALs.** TALs were masked with NHS-acetate and incubated at 37 °C for 30 min with either vehicle or forskolin (20 μM) plus IBMX (0.5 mM) in the presence or absence of H-89 (10 μM). One aliquot was not masked with NHS-acetate to measure basal surface NKCC2 (not shown). After treatment, suspensions were cooled down at 4 °C, and newly inserted NKCC2 was biotinylated. Surface NKCC2 was detected by Western blotting, and mean optical density was measured by densitometry. The difference between basal steady-state surface NKCC2 and NHS-acetate-masked samples was considered the NHS-acetate-masked NKCC2 fraction. Data are expressed as percent of the NHS-acetate-masked fraction over time as mean ± S.E. ($n = 6$; *, $p < 0.05$ *versus* vehicle).

tion of Epac agonist used was higher than those reported to activate Epac in renal tubules (10, 12, 13) and polarized epithelial cells. In addition, we observed that during PKA inhibition with H-89, the Epac-selective agonist decreased surface NKCC2 by 20% (data not shown), suggesting an inhibitory role of Epac in NKCC2 trafficking to the membrane that may be masked by low PKA activation. Together, our data indicate that PKA mediates cAMP-induced stimulation of steady-state apical surface NKCC2 in TALs.

The concentration of H-89 used here has been extensively validated for PKA inhibition (20, 30–33). In our experiments, 10 μM H-89 blocked 70–100% of the forskolin/IBMX effect in steady-state apical NKCC2 (Figs. 1 and 2). However, we observed only a partial blockade of cAMP-stimulated NKCC2 exocytosis (Fig. 6). We think that this is due to differences in the incubation time with H-89 in the two protocols. In the exocytic insertion protocol, TALs were warmed in the presence of both H-89 and forskolin/IBMX, whereas for steady-state surface NKCC2 measurements, the PKA inhibitor was preincubated with H-89 before increasing cAMP. It is possible that this shortens the time required for H-89 to maximally inhibit PKA. Alternatively, it is possible that a fraction of cAMP-stimulated exocytic insertion is mediated by a different cAMP-stimulated pathway.

We also observed constitutive NKCC2 insertion under basal conditions (Fig. 5), suggesting that trafficking of NKCC2 to the

apical membrane is a continuous dynamic process rather than an event triggered by cAMP. It is likely that constitutive endocytosis and recycling are involved in maintaining steady-state NKCC2 at the apical membrane. However, these processes appear not to be dependent on PKA activity because H-89 did not affect steady-state surface NKCC2 (Figs. 1 and 2) or the rate of exocytic insertion (Fig. 6). Although our data indicate that cAMP stimulates NKCC2 exocytosis, they do not exclude the possibility that cAMP affects endocytosis and recycling of NKCC2 and that these mechanisms also contribute to enhance apical membrane NKCC2 levels.

The protein targets by which PKA stimulates NKCC2 exocytosis are not known. Our previous data indicate that the SNARE (soluble *N*-ethylmaleimide-sensitive factor attachment protein receptor) family of proteins is involved in NKCC2 trafficking because the stimulation of surface NKCC2 by cAMP was blocked by tetanus toxin (6). This neurotoxin blocks vesicle fusion by cleaving the SNARE proteins VAMP-2 and VAMP-3, both of which are expressed and co-localize with NKCC2 in TALs (6). Several proteins that modulate SNARE-mediated exocytosis such as snapin (34), tomosyn (35), complexin (36), and Munc18 (37) mediate PKA-stimulated exocytosis. Thus, we speculate that PKA stimulates NKCC2 exocytosis by SNARE-dependent fusion and trafficking to the apical membrane of TALs. In addition to SNARE protein phosphorylation, rat NKCC2 possesses three predicted serine phosphorylation sites in its C terminus (4) that may serve as potential PKA targets. Although phosphorylation at these sites has not been described, N-terminal threonine phosphorylation is associated with enhanced activity (38), although the kinase involved (SPAK) appears to be unrelated to the cAMP pathway. The contribution of these pathways to NKCC2 exocytosis remains to be studied.

Acknowledgments—We thank Drs. Jeffrey L. Garvin and Mariela Mendez for thorough reading of the manuscript and comments.

REFERENCES

1. Nielsen, S., Maunsbach, A. B., Ecelbarger, C. A., and Knepper, M. A. (1998) *Am. J. Physiol. Renal Physiol.* **275,** F885–F893
2. Molony, D. A., Reeves, W. B., Hebert, S. C., and Andreoli, T. E. (1987) *Am. J. Physiol. Renal Physiol.* **252,** F177–F187
3. Hebert, S. C., Culpepper, R. M., and Andreoli, T. E. (1981) *Am. J. Physiol. Renal Physiol.* **241,** F412–F431
4. Gamba, G., Miyanoshita, A., Lombardi, M., Lytton, J., Lee, W. S., Hediger, M. A., and Hebert, S. C. (1994) *J. Biol. Chem.* **269,** 17713–17722
5. Gamba, G. (2005) *Physiol. Rev.* **85,** 423–493
6. Ortiz, P. A. (2006) *Am. J. Physiol. Renal Physiol.* **290,** F608–F616
7. Giménez, I., and Forbush, B. (2003) *J. Biol. Chem.* **278,** 26946–26951
8. Katsura, T., Gustafson, C. E., Ausiello, D. A., and Brown, D. (1997) *Am. J. Physiol. Renal Physiol.* **272,** F817–F822
9. Nielsen, S., Frøkiaer, J., Marples, D., Kwon, T. H., Agre, P., and Knepper, M. A. (2002) *Physiol. Rev.* **82,** 205–244
10. Yip, K. P. (2006) *Am. J. Physiol. Renal Physiol.* **291,** F882–F890
11. Ameen, N. A., Marino, C., and Salas, P. J. (2003) *Am. J. Physiol. Cell Physiol.* **284,** C429–C438
12. Honegger, K. J., Capuano, P., Winter, C., Bacic, D., Stange, G., Wagner, C. A., Biber, J., Murer, H., and Hernando, N. (2006) *Proc. Natl. Acad. Sci. U.S.A.* **103,** 803–808
13. Murtazina, R., Kovbasnjuk, O., Zachos, N. C., Li, X., Chen, Y., Hubbard, A., Hogema, B. M., Steplock, D., Seidler, U., Hoque, K. M., Tse, C. M., De Jonge, H. R., Weinman, E. J., and Donowitz, M. (2007) *J. Biol. Chem.* **282,** 25141–25151
14. Gapstur, S. M., Homma, S., and Dousa, T. P. (1988) *Am. J. Physiol. Renal Physiol.* **255,** F292–F300
15. Li, Y., Konings, I. B., Zhao, J., Price, L. S., de Heer, E., and Deen, P. M. (2008) *Am. J. Physiol. Renal Physiol.* **295,** F525–F533
16. Nielsen, S., Chou, C. L., Marples, D., Christensen, E. I., Kishore, B. K., and Knepper, M. A. (1995) *Proc. Natl. Acad. Sci. U.S.A.* **92,** 1013–1017
17. Snyder, P. M., Olson, D. R., Kabra, R., Zhou, R., and Steines, J. C. (2004) *J. Biol. Chem.* **279,** 45753–45758
18. Christensen, B. M., Zelenina, M., Aperia, A., and Nielsen, S. (2000) *Am. J. Physiol. Renal Physiol.* **278,** F29–F42
19. Nejsum, L. N., Zelenina, M., Aperia, A., Frøkiaer, J., and Nielsen, S. (2005) *Am. J. Physiol. Renal Physiol.* **288,** F930–F938
20. Hoffert, J. D., Fenton, R. A., Moeller, H. B., Simons, B., Tchapyjnikov, D., McDill, B. W., Yu, M. J., Pisitkun, T., Chen, F., and Knepper, M. A. (2008) *J. Biol. Chem.* **283,** 24617–24627
21. Yip, K. P. (2002) *J. Physiol.* **538,** 891–899
22. Mei, F. C., Qiao, J., Tsygankova, O. M., Meinkoth, J. L., Quilliam, L. A., and Cheng, X. (2002) *J. Biol. Chem.* **277,** 11497–11504
23. Kiermayer, S., Biondi, R. M., Imig, J., Plotz, G., Haupenthal, J., Zeuzem, S., and Piiper, A. (2005) *Mol. Biol. Cell* **16,** 5639–5648
24. Ares, G. R., Caceres, P., Alvarez-Leefmans, F. J., and Ortiz, P. A. (2008) *Am. J. Physiol. Renal Physiol.* **295,** F877–F887
25. Peng, Y., Amemiya, M., Yang, X., Fan, L., Moe, O. W., Yin, H., Preisig, P. A., Yanagisawa, M., and Alpern, R. J. (2001) *Am. J. Physiol. Renal Physiol.* **280,** F34–F42
26. Lee-Kwon, W., Kawano, K., Choi, J. W., Kim, J. H., and Donowitz, M. (2003) *J. Biol. Chem.* **278,** 16494–16501
27. Smith, C. B., and Betz, W. J. (1996) *Nature* **380,** 531–534
28. Cochilla, A. J., Angleson, J. K., and Betz, W. J. (1999) *Annu. Rev. Neurosci.* **22,** 1–10
29. Gaffield, M. A., and Betz, W. J. (2006) *Nat. Protoc.* **1,** 2916–2921
30. Dilly, K. W., Kurokawa, J., Terrenoire, C., Reiken, S., Lederer, W. J., Marks, A. R., and Kass, R. S. (2004) *J. Biol. Chem.* **279,** 40778–40787
31. Bhattacharya, A., Lakhman, S. S., and Singh, S. (2004) *J. Biol. Chem.* **279,** 37291–37297
32. Clayton, A., Holland, E., Pang, L., and Knox, A. (2005) *J. Biol. Chem.* **280,** 23451–23463
33. Perrotti, N., He, R. A., Phillips, S. A., Haft, C. R., and Taylor, S. I. (2001) *J. Biol. Chem.* **276,** 9406–9412
34. Chheda, M. G., Ashery, U., Thakur, P., Rettig, J., and Sheng, Z. H. (2001) *Nat. Cell Biol.* **3,** 331–338
35. Baba, T., Sakisaka, T., Mochida, S., and Takai, Y. (2005) *J. Cell Biol.* **170,** 1113–1125
36. Butterworth, M. B., Frizzell, R. A., Johnson, J. P., Peters, K. W., and Edinger, R. S. (2005) *Am. J. Physiol. Renal Physiol.* **289,** F969–F977
37. Liu, Y., Ding, X., Wang, D., Deng, H., Feng, M., Wang, M., Yu, X., Jiang, K., Ward, T., Aikhionbare, F., Guo, Z., Forte, J. G., and Yao, X. (2007) *FEBS Lett.* **581,** 4318–4324
38. Ponce-Coria, J., San-Cristobal, P., Kahle, K. T., Vazquez, N., Pacheco-Alvarez, D., de Los Heros, P., Juárez, P., Mũnoz, E., Michel, G., Bobadilla, N. A., Gimenez, I., Lifton, R. P., Hebert, S. C., and Gamba, G. (2008) *Proc. Natl. Acad. Sci. U.S.A.* **105,** 8458–8463